ADVANCED MATERIALS INTERFACES
www.advmatinterfaces.de

Plasma-Assisted Deposition of Silk Fibroin on Different Surfaces

Artem Arkhangelskiy, Devid Maniglio, Alessio Bucciarelli, Vamsi K. Yadavalli, and Alberto Quaranta*

The development of simple and versatile methods for the deposition of biocompatible coatings to protect or functionalize a range of materials with different shapes is an important challenge. In this study, a versatile, room-temperature process is presented for the deposition of silk fibroin on different materials viz., glass, polyethylene terephthalate, Ti alloy, and poly(dimethylsiloxane). Coating with thin fibroin films is achieved using an atmospheric plasma torch, wherein a silk-fibroin aerosol solution is used as the working gas. The method consists of two sequential processes: plasma modification of the surface, followed by plasma-assisted deposition. This allows enhanced adhesion of the protein to the underlying surfaces, and the deposition even on non-planar and flexible substrates. The deposited films are characterized by optical microscopy, atomic force microscopy, and scanning electron microscopy. Primary and secondary structures of the surface-attached fibroin films are investigated by Fourier transform infrared spectroscopy. The proposed approach offers a tunable and controllable strategy for the controlled deposition of proteins on complex surfaces, for a wide range of biomedical and technological applications, including dentistry and bioelectronics.

1. Introduction

Silk fibroin is a natural biopolymer that has been successfully proposed as a biomaterial in tissue engineering, biosensing, and more generally, in biomedical applications due to its unique mechanical and structural properties, and its positive interaction with biological environments.[1–3] The mechanical properties of fibroin can be easily tuned by controlling its crystalline structure (specifically, β-sheet content), which also has a direct impact on its degradation rate. The combination of these properties, together with its high thermal stability and processability by diverse fabrication techniques, make silk fibroin suitable for the production of biocompatible shapes and forms. Various solid constructs, sponges, hydrogels, membranes, micro/nano particles, and films have been reported to date.[4–8] One of the most interesting uses of silk fibroin lies in the realization of bioactive coatings. This allows the translation of the positive biological interactions and properties of fibroin to different surfaces, while preserving the intrinsic properties of the bulk (underlying) materials.[9–11] For optimal performance, silk fibroin coatings should possess not only biological properties, but also good mechanical and chemical stability, together with strong adhesion to the underlying surface.

The most widely used technique to produce thin and ultrathin coatings on different substrates is layer-by-layer (LbL) deposition.[12,13] This technique can form films from 1 nm to 1 µm, via the alternate layering of oppositely charged polyelectrolytes. In the case of silk fibroin, the use of stepwise dipping – a variation of standard LbL[14] – and spin-assisted LbL[15] has been used to form ultrathin layers (1–100 nm) by exploiting hydrophobic interactions. In the former, fibroin is deposited by immersing the substrate into an aqueous solution followed by washing and drying steps. In the latter, fibroin films are formed by spin-casting of silk-ionic-liquid solutions, and subsequently treated with methanol or water. More typically, however, pre-treatment

A. Arkhangelskiy, Prof. A. Quaranta
Department of Industrial Engineering
University of Trento
Via Sommarive 9, Trento, TN 38123, Italy

The ORCID identification number(s) for the author(s) of this article can be found under https://doi.org/10.1002/admi.202100324.

DOI: 10.1002/admi.202100324

Prof. D. Maniglio
BIOtech Center for Biomedical Technologies
Department of Industrial Engineering
University of Trento
Via Sommarive 9, Trento, TN 38123, Italy
E-mail: devid.maniglio@unitn.it
Dr. A. Bucciarelli
CNR-Nanotec
Institute of Nanotechnology
National Council of Research c/o Campus Ecotekne—Università del Salento
via Monteroni, Lecce, Lecce 73100, Italy
Prof. V. K. Yadavalli
Department of Chemical and Life Science Engineering
Virginia Commonwealth University
601 W Main Street, Richmond, VA 23284, USA

and post-treatment procedures are required. Pre-treatment procedures consist of physical/chemical modifications of the target surface. Methanol/water deep cleaning, or oxygen plasma and ultraviolet (UV)/O_3 surface activation treatments have been reported to be effective in enhancing the adhesion of silk fibroin films to various substrates.[16,17] Moreover, preparation of silk fibroin films with nanotopography using poly(dimethylsiloxane) (PDMS) molds was reported as a prospective method for wound healing applications.[18] For post-treatment, a combination of micro/nanopatterning and temperature, methanol/water vapor exposure, or UV irradiation have resulted in controllable structural transitions of silk fibroin to the more stable crystalline form.[19] Another promising method for tunable deposition of silk fibroin is pulsed laser deposition (PLD).[20,21] A neat ablation target produced by pressing fibroin powder, is fixed in a vacuum chamber and then irradiated by a laser beam to induce ablation. Film thickness is controlled by deposition time, while the β-sheet content is controlled by the ablation conditions. The need for vacuum chambers, and the limited yield due to the small deposition area, makes this method difficult to apply for wide-scale applications. Silk fibroins films obtained by the above methods are stable and have good mechanical properties, which can be controlled by changing the secondary structure through physical crosslinking, inducing β-sheet molecular interactions. However, limitations include the difficulty in controlling film thickness, and the exclusion of controlled assembly on large or flexible substrates, or those with complex geometry such as screws or pins.

Some of the most challenging substrates for silk fibroin deposition are metals, because of poor adhesion due to low wetting of fibroin, as well as complex surface topography which makes the intimate contact of molecules difficult.[11] This limitation can be overcome by taking advantage of the electrical conductivity of metals. Since silk fibroin has a polyampholyte nature in water, it can be subjected to electrophoresis and guided to assemble on metal anodes under an electric field.[22,23] Also, this technique can be suitable for the deposition of silk fibroin nanospheres for drug delivery application, providing better cell response and enhanced drug release.[24] While fibroin can be deposited on metallic substrates, non-conductive materials such as polymers cannot be coated using this method. This includes flexible polymers and elastomers, such as PDMS, whose easy deformability can induce delamination and cracking of the coating. To overcome this limitation, electrospinning of a nanometer fibroin fiber mesh was proposed.[25] Electrospinning variables are controlled in order to have suitable adhesion after tensile testing. However, the high content of polyethylene oxide (PEO) is needed to obtain the required viscosity for electrospinning, and the difficulty in controlling thickness can limit applications. Another promising method for the deposing of silk fibroin on PDMS is the combination of dip-coating with electrospinning.[16] Good adhesion is provided by the plasma pretreatment of PDMS surface, while the thickness is controlled because the deposition of electrospun silk fibers is randomized on the wet surface after dip-coating. Despite the progress in silk fibroin deposition methods, the deposition on flexible substrates and metals continues to be limited by problems of delamination, and a lack of a universal method for depositing silk fibroin coating on a wide range of materials with different shapes.

Here we demonstrate a versatile method for forming silk fibroin thin films on diverse substrates via a direct, controlled atmospheric plasma-assisted deposition process. Compared to other techniques, this method is simple and allows the fabrication of silk fibroin coatings on a range of substrates—from glass and Ti alloy, to polyethylene terephthalate (PET) and PDMS. Moreover, the deposition is carried out at room temperature and atmospheric pressure without the need for specialized process vacuum chambers. Improved adhesion strength allows avoiding any pre-treatment methods, reducing the time and the complexity of the production of the silk fibroin films. An aerosol realized from an aqueous fibroin solution injected in a cold plasma torch enables simultaneous surface activation and protein deposition. The structure of the fibroin coating can be controlled by the carrier gases used, as well as the power of the radiofrequency (RF) used to sustain the plasma. We show how this deposition can be performed on both planar and non-planar surfaces (e.g., screws). Various characterization methods of the coatings are presented—Attenuated total reflectance-Fourier transform infrared spectroscopy (ATR-FTIR) was used to investigate the structure of the deposited films. Atomic force microscopy (AFM) and scanning electron microscopy (SEM) were used to study the conformation and morphology of the coating. The stability of the films was observed in phosphate-buffered saline (PBS) at 37 °C following ultrasonication treatment in water. This low-temperature plasma process can therefore provide a valuable tool to form bioactive coatings on a range of substrates.

2. Results and Discussion

Plasma processing is a promising and fast-developing manufacturing tool in industrial and biomedical engineering applications.[26,27] Plasma (ionized gas) consists of excited species, electrons, ions, radicals, neutral molecules, as well as short-wave radiation. This provides an effective, low temperature, and environmentally friendly method for surface modification. When the plasma begins to interact with a surface, changes in wettability, surface energy, chemistry, and even surface morphology may be obtained. By tuning plasma parameters and use of suitable gases, a controllable and reproducible deposition can be applied to metals, polymers, or ceramics. Moreover, plasma can provide sterilization of the surface, which may have an impact on biomedical applications. In general, plasma methods can operate at room temperature and require less energy than wet chemical methods, with no changes in the material's bulk properties. For instance, an atmospheric pressure plasma jet (APPJ) can produce a stable plasma plume without using expensive vacuum systems. The APPJ can be used for a range of processes such as surface cleaning, etching, functionalization, plasma polymerization/deposition, or plasma-graft polymerization.[28]

Plasma polymerization/deposition provides thin, uniform, and homogeneous layers of different materials with strong adhesion to a wide range of substrates.[29–31] Such strong adhesion accrues due to covalent bonds between functionalized substrate and deposited material, preventing delamination.[32–35] In order to evaluate the possibility of plasma deposition of silk fibroin using atmospheric pressure plasma torch (jet)

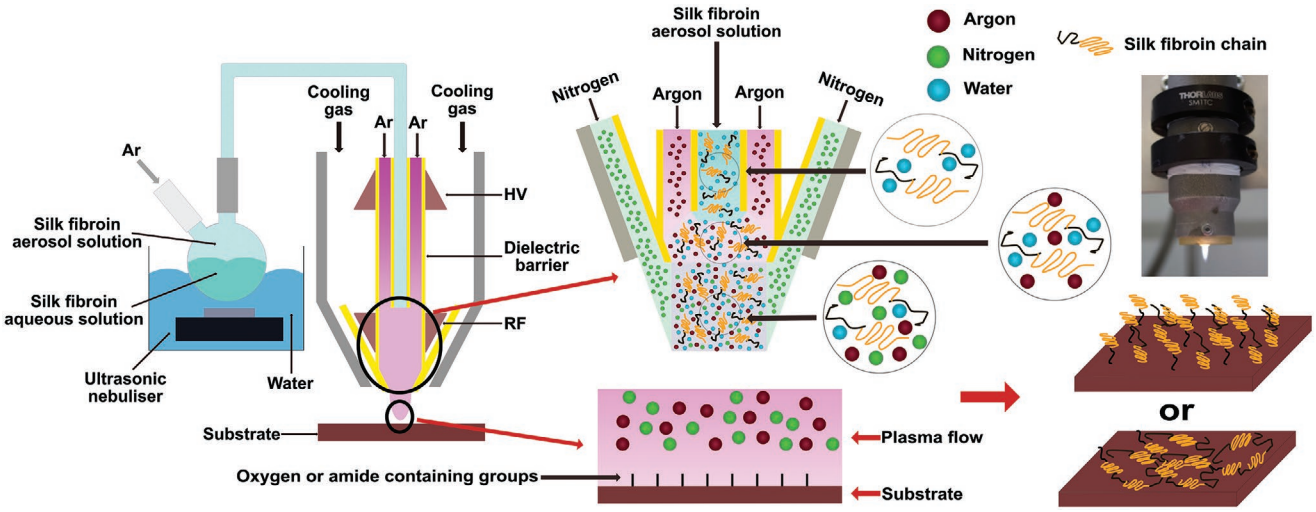

Figure 1. Schematic illustration of the deposition process: silk fibroin solution is vaporized using an ultrasonic nebulizer. The aerosol is injected into the plasma torch gas line, followed by plasma modification of the surface and deposition. Details of the process are presented in the experimental section.

on different materials, glass, PET, PDMS, and Ti6Al4V alloy were used as model substrates. Glass was used as a reference material due to insulation properties and smooth surface, while Ti6Al4V alloy was chosen as a biocompatible alloy and conductive material. PDMS and PET were chosen as polymeric materials (elastomeric and thermoplastic, respectively).

Plasma deposition of the silk fibroin results from the combination of different processes. Plasma sputtering (cleaning) of the substrate, which occurs when excited species generated from an inert gas (Ar) collides with the solid. This process not only cleans, but also sterilizes the surface. Further, during sputtering, the excited species react with the substrate surface and induce functionalization with oxygen and amide-containing groups.[35] In the plasma polymerization of silk fibroin, two simultaneous competitive processes take place. In the first phase silk fibroin is deposited on the substrate then the etching action of plasma starts to erode the formed film. Only when the deposition is predominant over etching, the thickness growth is promoted. We also hypothesize that during deposition, plasma may affect the silk-fibroin secondary structure due to the presence of free argon and N_2/O_2. Initially, the silk fibroin aerosol solution is affected by argon plasma inside the plasma gas line, changing the secondary structure and charge of fibroin chains. Then this plasma flows with the fibroin aerosol solution mixed with nitrogen (cooling gas) and is deposited on the substrate (**Figure 1**). We assume that during all steps of deposition, dehydration of the structure occurs because of the use of a dry inert atmosphere. Moreover, plasma continues to influence the already deposited layer also during deposition. Depending on the substrate and presence of already deposited layers, silk fibroin can attach and orient differently because of the continuous change at the surface and the reactive species distribution.

2.1. Optical Images of Silk Fibroin Coatings

The coatings obtained on glass, PET, PDMS, and Ti6Al4V can be observed in **Figure 2**. Deposition parameters were kept the same for all materials: power 10 W, the distance between substrate and plasma torch ≈6 mm, speed of the torch – 100 mm min^{-1}. Low power was set in order to reduce the influence on the etching mechanism. 10 W power is the lowest power limit to maintain a stable plasma plume. It is worth noticing that the plasma deposited silk fibroin stripes are homogeneous on all substrates with a width around 1 cm, which corresponds to the diameter of the region irradiated by the plasma plume. While the deposition on flat substrates was obtained with ease, this technique can also be applied to more complex geometries. In order to test the deposition capability on a non-planar surface, a Ti6Al4V cylindrical pin was put in rotation and exposed to the plasma torch (Figure 2d). Due to the presence of free charge carriers, plasma is electrically conductive[36] and exhibits different behavior on conductive or non-conductive substrates. On the Ti6Al4V surface, the current induced by plasma flows through the sample inducing zero charge accumulation on the top of the surface. In contrast, on insulating substrates (glass, PET, PDMS), the charge can accumulate on the top of the surface.

In order to visualize the silk fibroin on the transparent surfaces, the protein was stained using crystal violet which provides good contrast, allowing easier observation. Close-ups of these surfaces using optical microscopy are shown in the Supporting Information (Figure S1, Supporting Information). Samples were stretched and bent in order to observe the preliminary strength of adhesion. PDMS and PET samples (Figure 2a,b) show uniform coatings with no significant cracks or delamination. A slight difference in morphology can be explained by the effect of plasma or different optical properties of materials. For determining the mechanism of building-up of the silk fibroin layers, an SEM cross-section image was used, as shown in **Figure 3**a, with the sample obtained using 80 runs (resulting in a film thickness of about 6 µm). The homogeneous and uniform structure of the films is clearly observed, showing that each pass does not create growth through a layered structure. This has implications in the homogeneity and strength of the deposited bioactive film on the substrate.

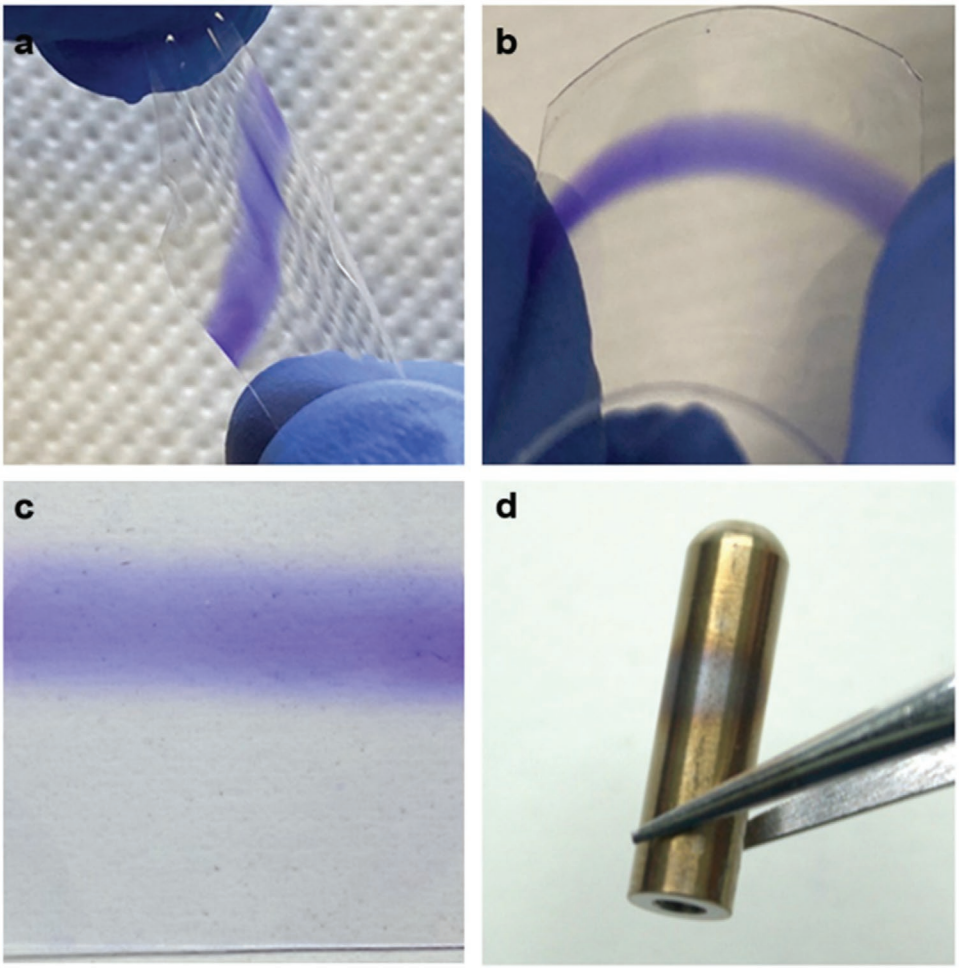

Figure 2. Images of coated samples on a) PDMS, b) PET, c) glass, and d) Ti6Al4V cylindrical pin. Blue coloration is due to the crystal violet solution.

One of the most promising applications of plasma deposited silk fibroin is in the surface modification of complex, non-planar surfaces. For instance, a screw with multiple threads and crevices, can make uniform deposition via traditional methods challenging. While a round pin was shown above, we show that this technique is adaptable even for such geometries. A silk fibroin coating was deposited on a Ti6Al4V screw (Lincotek Trento S.p.A) as shown in Figure 3b. Figure S2, Supporting Information, shows the SEM images of the unmodified and modified screws confirming the deposition. Coated samples are uniform with a similar surface morphology to the cross-section image shown in Figure 3a. The deposition on a curved surface can lead to a difference of thickness owing to a differential etching mechanism due to variations in height between the plasma nozzle and surface. To avoid this effect, when the sizes of curved parts are bigger in comparison with the diameter of the plasma plume, it is necessary that the plasma torch follows the geometry of the part during its scan. When the diameter

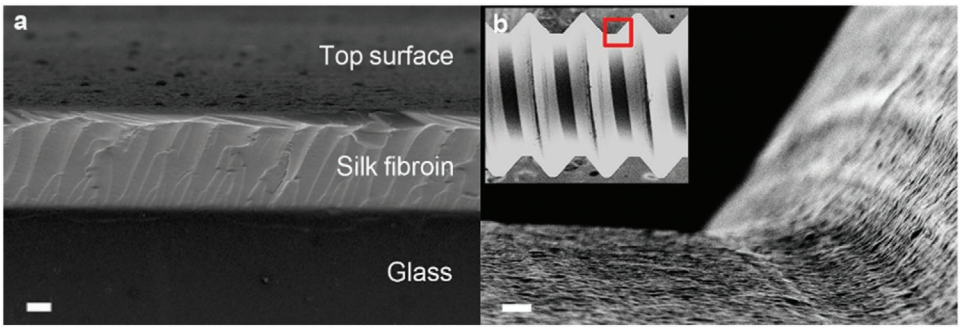

Figure 3. a) SEM image showing the cross-section of deposited silk-fibroin on glass. Scale bar = 1 µm. b) SEM image showing deposited silk fibroin coating of Ti6Al4V screw. Scale bar = 2 µm.

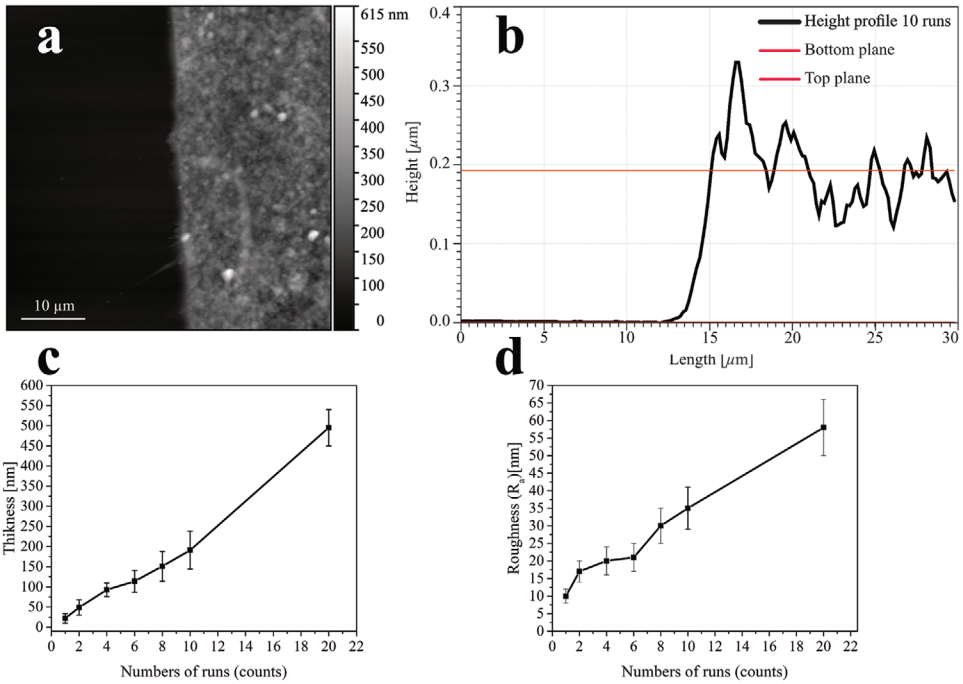

Figure 4. a) AFM image of film edge. Scale bar = 10 µm. b) Height profile across the film edge. c) Thickness dependence of plasma deposited silk fibroin films on the number of runs on the glass substrate (power–10 W, speed–100 mm min^{-1}). d) Roughness dependence of plasma deposited silk fibroin films on the numbers of runs on a glass substrate (power–10 W, speed–100 mm min^{-1}).

of the plasma plume is bigger than the sizes of curved parts, the use of multiple runs can minimize the variation in surface thickness of the coatings.

2.2. Microstructure of the Silk Fibroin Coatings

The microstructure of the deposited fibroin films was characterized using AFM in order to understand the conformation and growth on different substrates as shown in **Figure 4**. The AFM was used to observe the interface of the film with the underlying substrate to observe the film edge and determine film thickness. The thickness obtained from the cross-section was 191 ± 47 nm (Figure 4a,b). The thickness of the plasma deposited silk fibroin on glass substrate increases linearly with the number of runs, confirming LbL deposition (Figure 4c). It may be expected that after deposition of a certain thickness of silk fibroin layer, the plasma plume does not reach the substrate, minimizing etching mechanism and promoting deposition process, which explains the high growth from 190 (10 runs) to 495 nm (20 runs). Standard deviation values are correlated with the surface roughness values (Figure 4d). AFM scans showing the nanoscale surface morphology are presented in Figure S3, Supporting Information, which show almost the same lateral granular sizes in comparison with standard LbL deposition techniques with lateral granular sizes in the order of micrometers. It is worth noticing that while the granular size is the same, the surface roughness (R_a) is much higher, 35 nm ± 6 nm in comparison with 1.34 ± 0.12 nm for stepwise deposition,[14,15] in which silk fibroin solution was obtained by dissolving silk fibroin in LiBr. While, silk films obtained by casting from solution, prepared by dissolving degummed silk in $CaCl_2$/H_2O/C_2H_5OH, also show lower values.[37] Such high values of surface morphology of plasma deposited silk fibroin films can be explained owing to the uneven etching mechanisms occurring during plasma deposition. Figure S3, Supporting Information, shows the surface morphology of the silk films on glass, PDMS, PET, and Ti6Al4V. Glass, PDMS, and PET show almost the same R_a (45 ± 9 nm, 43 ± 10 nm, 41 ± 9 nm) and lower values with respect to the Ti6Al4V, for which R_a is 71 ± 32 nm. Such an increase in roughness can be explained by the higher roughness of bare Ti6Al4V. Moreover, the granular sizes on all substrates are the same, proving that the substrate itself has a low influence on the deposition process. We also assume that silk-fibroin can orient itself on a conductive substrate in the direction of the conductive path. This can be hypothesized owing to the formation of microcavities during polishing, promoting the orientation of silk fibroin (Figure S3d, Supporting Information).

2.3. FTIR Analysis and Structure Reconstruction

Understating the influence of the plasma on the structure of the deposited silk fibroin films is important for tailoring high-impact material functionalization. Different depositions were performed using both nitrogen and compressed air as cooling gases, at power values, ranging from 10 to 25 W. As noted earlier, 10 W is the minimum value at which the plasma is stable and reproducible, while 25 W is the upper limit at which deposition can occur. At higher power, etching processes play a much larger role than deposition processes, perverting film growth.

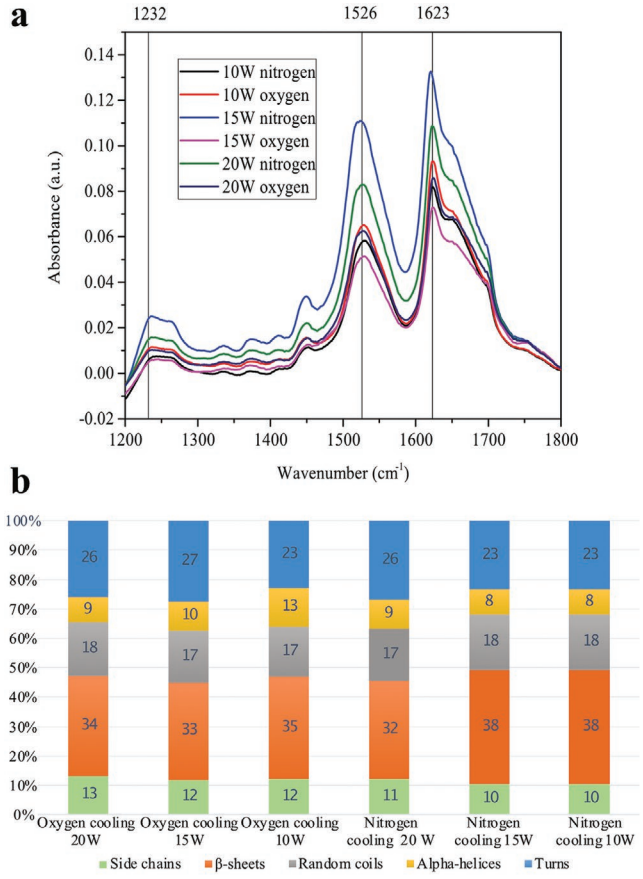

Figure 5. a) ATR-FTIR spectra of a deposited silk-fibroin film. To make film homogenous for the analysis, the following deposition parameters were used: number of runs–16 (3 runs at 100 mm min^{-1}, then 5 runs at 300 mm min^{-1}, and then 8 runs at 500 mm min^{-1}), substrate–glass, distance from the substrate–6 mm. b) Quantitative data of secondary structure of deposited silk fibroin films.

Compressed air was chosen in order to evaluate the changes of silk fibroin structure in an oxygenated environment. With compressed air cooling, oxygen molecules tend to neutralize free electrons from the plasma, making it less effective from a physicochemical point of view. ATR-FTIR measurements were used to understand the structure of the plasma deposited silk-fibroin films. **Figure 5**a shows the amide I absorption band at 1623 cm^{-1}, amide II absorption band at 1526 cm^{-1}, and amide III absorption band at 1232 cm^{-1}. A strong peak at 1623 cm^{-1}, which is a characteristic of antiparallel β-structures, with the shoulder at 1648 cm^{-1} is a common feature of deposition methods.[17,18] In order to evaluate the secondary structure of deposited silk-fibroin films, Fourier self-deconvolution and peak fitting were used (Figure S4, Supporting Information). The area of fitted peaks is correlated with a secondary structure. The data of the relative ratios are reported in Figure 5b and Table S1, Supporting Information. From the analysis, plasma deposited silk-fibroin deposited on glass has a high quantity of β-sheets (32 to 38%), side chains (10 to 13%) and α-helix (8–11%), and a low quantity of random coils (17 to 18%) and turns (23 to 27%).

This minor difference in quantity leads us to hypothesize that changing power and cooling gas have a lower influence on the secondary structure of silk fibroin coating. To determine the effect of the atmospheric plasma on silk fibroin, the secondary structure of the obtained coatings was compared with data on fibroin films previously reported.[37] The plasma coatings exhibit similar content of β-sheets and α-helix, but a lower percentage of random coils compared to silk fibroin films formed by solution casting in polystyrene petridishes without post-treatment (32% β-sheets, 8% α-helix, and 30% random coils). The same films, after methanol annealing, evidenced β-sheets increase to 52%, with a strong reduction of random coils (18%). In these films, the strong reduction of amorphous regions (random coil) is at the base of their stability in water, similar to plasma deposited silk fibroin coatings. We assume that crystalline regions (β-sheets structure), due to their stability, are less affected by plasma treatment.[38–41] It is also evident that plasma can modify and change the structure of the silk protein, inducing conversion of random coils into side chains. In Argon gas, which creates an inert atmosphere in the deposition area, the formation of β-sheets might be induced by the dehydration of the structure.[10] The structure can also be influenced by the substrate, like glass, where β-sheets formation is favored.[42] Thus, depending on the substrate selected, these parameters can be tuned in order to achieve optimal film coatings.

2.4. Adhesion Strength and Stability of the Coatings in Aqueous Environments

The stability and adhesion of the fibroin layer to the underlying substrate is a crucial point in evaluating various deposition techniques for flexible applications. Images of the samples before and after soaking in PBS buffer over 2 weeks are shown in **Figure 6**a and Figure S5, Supporting Information. All samples showed a stable (undissolved) silk fibroin coating. This is presumably due to the high crystallinity of the structure (over 30% β-sheets) and low content of random coils (17–18%).[43] It may be noted that the fading of the blue color of the films is merely due to washing out of the crystal violet solution. We also assume that owing to dehydration and the inert atmosphere of the fabrication process, the deposited films are already very dry, allowing them to be stable in air for a long period of time without any degradation. Meanwhile, we expect that the deposited fibroin will undergo proteolytic degradation, following pathways already described in the literature.[44,45] Plasma deposited films, therefore, showed good adhesion to the underlying surface also after attaching and detaching adhesion tape (Figure 6b). Lower adhesion to the PDMS substrate might be due to low wettability, high stretchability of the material, and plasma behavior on it. PDMS is a soft material that might be more affected by plasma, inducing rougher morphology onto PDMS during deposition, with micro or even nano delamination regions. While immersing the sample in crystal violet aqueous solution, water might pass between the silk fibroin film and the PDMS substrate, reducing adhesion. Changing the cooling gas from nitrogen to compressed air could lead to better adhesion. Firstly, increasing oxygen content in plasma flow might induce better oxidation of the surface and increasing wettability. As noted earlier, oxygen molecules make plasma less effective from a physicochemical point of view, reducing

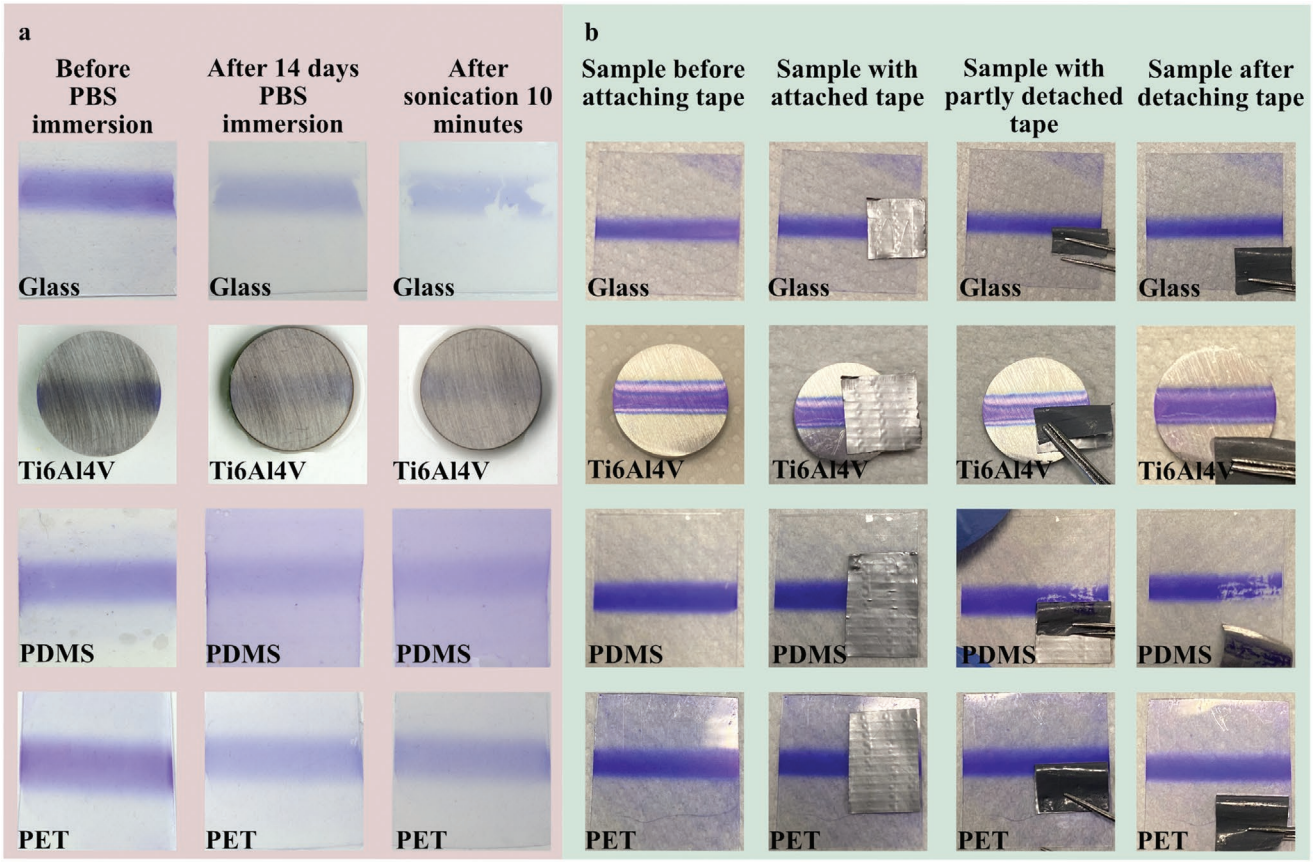

Figure 6. a) Photos of the silk fibroin films observed in buffer solution for 2 weeks at 37 °C following ultrasonication treatment in water. All photos were made in wet condition. b) Photos of the silk fibroin film before and after the peeling test using adhesive tape. Before the test, samples were immersed in a crystal violet solution and dried with nitrogen.

the etching mechanism. This might lead to less micro-delamination regions. PET is less affected by the plasma due to hardness, better wettability, and inability to stretch. These factors reduce delamination regions and enhance adhesion in comparison with PDMS. We assume that, during deposition, the plasma charges both the substrate surface and silk-fibroin aerosol solution, increasing the electrostatic interaction.[46,47] In the meantime, the plasma might induce surface modification by itself. On the glass surface, the plasma results in the formation of OH groups on the surface, arising from the water in the fibroin aerosol, while the presence of nitrogen inserts amide groups on the surface.[48]

On PDMS, the plasma increases the presence of polar groups on the surface, such as SiO_2, Si—OH and $Si—CH_2OH$, while the nitrogen gives rise to the formation of NH_2 groups.[49–51] In the case of PET, the plasma induces the formation of oxygen functional groups such as hydroxyl and carboxyl groups on the surface,[52] while nitrogen can induce the formation of amide functional groups.[53] Plasma deposition on titanium alloys might increase the thickness of the oxide layer, promoting surface hydration, while also inducing the formation of oxygen functional groups on the top of the surface.[54] All these factors can promote the formation of the covalent bonding between protein and surface, thereby increasing the adhesion strength on these surfaces.

Plasma-assisted deposition of silk fibroin polymer combines the advantages of plasma processes and silk fibroin as a natural polymer. It allows the deposition of uniform and homogeneous silk fibroin films on metals with complex geometry, glass, and flexible materials such as PET and PDMS. It is notable that, on the chosen substrates, the different surface properties and interactions with plasma have a low impact on the conformation of silk fibroin. Plasma deposition provides a controllable and tunable deposition process with linear growth in thickness. Due to the etching process, the roughness of the films is quite high, which can be an advantage for biological applications. Moreover, this atmospheric plasma represents a benign process, characterized by low power and low temperature, but efficient deposition. A minimal change of the protein structure is obtained in comparison to other techniques such as film casting from aqueous solution and β-sheet induction by methanol exposure. Due to the insolubility and flexibility of the deposited silk fibroin films, no post-treatment procedures are needed. The most interesting and promising advantage of this method in flexible applications is the outstanding adhesion between substrate and silk fibroin film. Covalent bonding with enhanced electrostatic interaction provides no delamination after bending of PET and PDMS substrate. The peeling test also shows good adhesion with excellent stability in PBS solution suitable for biomedical applications. These silk fibroin

coating might be used for tissue engineering, especially in the field of implants and implantable devices.[55–57] Due to the high transparency and low thickness of the films, various optical applications can also present opportunities for further investigation.[58,59]

3. Conclusion

Here, we have demonstrated for the first time, the deposition of silk fibroin by using a room temperature, atmospheric plasma torch on diverse substrates: glass, PDMS, PET, and Ti6Al4. This method provides strong adhesion of the fibroin protein film with the ability to deposit even on non-planar with complex geometry surfaces. The deposition consisted of two main processes: plasma modification of the substrate with the formation of functional groups, followed by deposition of the protein. The deposition of silk fibroin was confirmed by ATR-FTIR, which showed the high β-sheet formation and low content of random coils due to dehydration, and the effect of plasma. Plasma modification enhanced the adhesion of the silk fibroin to the substrate, which may be explained by improved electrostatic interaction and induction of covalent bonds between functional groups formed on the substrate surface and the protein. These films were stable in PBS for 2 weeks, and even after treatment in a sonication bath. The simplicity and reproducibility of the plasma deposition process can therefore enable this method for different surface modification applications for bioelectronics, medical devices, and implants. Further studies are currently being conducted to use this technique for depositing other natural biopolymers, such as chitosan and collagen, to form multifunctional layered coatings.

4. Experimental Section

Preparation of Silk-Fibroin Solution: Silk cocoons were imported from Thailand (Chul Thai Silk Co., Phetchabun, Thailand). Extraction and purification of silk fibroin were conducted using an adapted version of a well-known protocol.[6] Briefly, cocoons of *B. mori* were boiled two times for 90 min in an aqueous solution of Na_2CO_3 (Sigma-Aldrich), first time, the concentration of the salt was set at 1.1 g L^{-1}, the second time at 0.1 g L^{-1}. The resultant fibroin fibers were gradually taken at room temperature and rinsed three times with distilled water to carefully remove the residual sericin and wax. The extracted silk fibroin was then dissolved in 9.3 M LiBr (Sigma-Aldrich) solution at 65 °C for 4 h, yielding a 20% (weight/volume) solution. This solution was dialyzed against distilled water using a dialysis cassette (MWCO 3500, Pierce, 0.5–3 mL) at room temperature for 3 days to remove the salt. To remove impurities, the solution was then filtrated with a glass filter. The final concentration of silk fibroin aqueous solution, tested by optical method evaluating the absorbance at 280nm (Nanodrop, ThermoFisher), was approximately 5–5.5% (wt./vol.). To avoid breakage of the plasma torch, and to allow the stable formation of aerosol solution, the silk fibroin stock solution was diluted to 0.1–0.2% (wt./vol.) deionized (DI) water.

Plasma Torch: A commercially available atmospheric plasma torch (Stylus Plasma Noble, Nadir Tech SRL)[60] was used for silk fibroin plasma deposition (Figure 1). The torch has 3 main components: a high voltage (HV) generator, an RF generator, and a gas system. The HV generator provided ignition of the precursor gas and extraction of the plasma flow from the ignition region to the stylus tip. The plasma density was controlled by the RF generator that can be adjusted through an impedance matching circuit by the user. The gas system consisted of three concentric channels: the plasma channel where the plasma was generated, the cooling channel which prevents overheating of the system, and a capillary channel to inject vapor or aerosol precursors into the generation region.

Plasma Deposition of Silk Fibroin: The plasma deposition of thin films was obtained as follows. The plasma torch was adjusted in order to get a stable plasma plume. The diluted silk fibroin solution was sonicated in a glass vial using an ultrasonic nebulizer to obtain an aerosol solution. The schematic illustration of the setup is as shown in Figure 1. The aerosol was then injected into the plasma torch gas line via Ar gas, which was used as a precursor (working) gas. The working gas (aerosol solution with Ar) then was injected into the plasma area. The plasma area was highlighted in purple in the principal alumina tube, where the Ar was supplied. Then the working gas passed through the plasma region to the torch exit with the plasma plume, where it mixes with a cooling gas followed by the deposition on chosen substrate. Deposition was carried out on different substrates: glass, PET, PDMS, and Ti alloy (Ti6Al4V). The parameters of deposition were kept the same for all materials to compare the deposition process on each. The flow of Ar in the plasma channel was 5 standard liter per minute (slm). The flow of N_2 or compressed air in the cooling channel was 15 slm and the flow of Ar in the precursor channel, which drives the aerosol solution to the plasma head, was 0.3 slm. For deposition, the substrates were placed on a plate mounted on a three-axis stage moving at different speeds: 100, 300, and 500 mm min^{-1}. One linear deposition with the path through the entire samples was set as one run.

Physical and Chemical Characterization: Images were obtained by optical microscopy (Zeiss Axiotech 100). In order to render the protein films visible to the eye, they were immersed in 2% crystal violet solution for 5 min. High-resolution images were obtained using a Supra 40 (Zeiss) field emission electron microscope (FESEM). Samples were coated with 4 nm Pt80Pd20 alloy by plasma sputtering. Surface topography was investigated using NT-MDT Solver Pro AFM in semi-contact mode. The image of the edge of the silk fibroin film was obtained by applying a mask on the substrate to control deposition. The top and bottom planes were fitted using Gwyddion software to calculate the profile. FTIR was performed in the range 400–3800 cm^{-1} with a Nicolet Avatar 330 spectrometer to determine the percentage of the different secondary structures in the I and II Amide region. FTIR spectra were collected in ATR mode, mediating 64 scans with a resolution of 2 cm^{-1}. The secondary structure of plasma deposited films was investigated by deconvolution of the amide I spectra (1590–1710 cm^{-1}).[61,62] A Fourier self-deconvolution algorithm[63] was used to individualize peak position. Fitting of the peaks was performed with a Gaussian function to minimize χ^2. The percentage area of each peak was related to the different secondary structures (random coil, beta-sheets, turns, α-helix, and side chains). In order to investigate the physical stability of silk fibroin films on glass, Ti6Al4V, PDMS, and PET samples were placed in PBS solution (pH 7.4) for 2 weeks at 37 °C, followed by treatment in a sonication bath for 10 min. Adhesion strength was evaluated by peeling test using adhesive tape (LUX Gewebeband Universal).

Supporting Information

Supporting Information is available from the Wiley Online Library or from the author.

Acknowledgements

This project has received funding from the Italian Ministry for Education, University, and Research (MIUR) through the "Departments of Excellence" program.

Conflict of Interest

The authors declare no conflict of interest.

Data Availability Statement

Research data are not shared.

Keywords

atmospheric pressure plasma, plasma deposition, poly(dimethylsiloxane), silk fibroin, thin films, Ti6Al4V alloy

Received: March 2, 2021
Revised: May 3, 2021
Published online:

[1] H. Tao, D. L. Kaplan, F. G. Omenetto, *Adv. Mater.* **2012**, *24*, 2824.
[2] C. Vepari, D. L. Kaplan, *Prog. Polym. Sci.* **2007**, *32*, 991.
[3] N. Jaramillo-Quiceno, A. Restrepo-Osorio, *J. Appl. Polym. Sci.* **2020**, *137*, 48505.
[4] A. Bucciarelli, R. K. Pal, D. Maniglio, A. Quaranta, V. Mulloni, A. Motta, V. K. Yadavalli, **2017**, *201700110*, 1–9.
[5] D. Maniglio, W. Bonani, C. Migliaresi, A. Motta, *J. Biomater. Sci., Polym. Ed.* **2018**, *29*, 491.
[6] D. N. Rockwood, R. C. Preda, T. Yücel, X. Wang, M. L. Lovett, D. L. Kaplan, *Nat. Protoc.* **2011**, *6*, 1612.
[7] M. J. J. Liu, S. M. Chou, C. K. Chua, B. C. M. Tay, B. K. Ng, *Med. Eng. Phys.* **2013**, *35*, 253.
[8] K. Tsuchiya, N. Ifuku, Y. Koyama, K. Numata, *Polym. Degrad. Stab.* **2019**, *160*, 96.
[9] B. Marelli, M. A. Brenckle, D. L. Kaplan, F. G. Omenetto, *Sci. Rep.* **2016**, *6*, 25263.
[10] X. Wang, X. Hu, A. Daley, O. Rabotyagova, P. Cebe, D. L. Kaplan, *J. Controlled Release* **2007**, *121*, 190.
[11] Y. Guo, J. Guan, H. Peng, X. Shu, L. Chen, H. Guo, *Mater. Des.* **2019**, *175*, 107825.
[12] G. Decher, *Science* **1997**, *277*, 1232.
[13] H. Ai, S. A. Jones, Y. M. Lvov, *Cell Biochem. Biophys.* **2003**, *39*, 23.
[14] X. Wang, H. J. Kim, P. Xu, A. Matsumoto, D. L. Kaplan, *Langmuir* **2005**, *21*, 11335.
[15] C. Jiang, X. Wang, R. Gunawidjaja, Y. -H. Lin, M. K. Gupta, D. L. Kaplan, R. R. Naik, V. V. Tsukruk, *Adv. Funct. Mater.* **2007**, *17*, 2229.
[16] A. P. Shete, A. A. Nisal, A. K. Lele, *WO2018173074*, **2018**.
[17] C. Wang, H. Fang, X. Qi, C. Hang, Y. Sun, Z. Peng, W. Wei, Y. Wang, *Acta Biomater.* **2019**, *91*, 99.
[18] Y. Luo, K. B. Kang, R. Sartaj, M. G. Sun, Q. Zhou, V. H. Guaiquil, M. I. Rosenblatt, *Sci. Rep.* **2021**, *11*, 8168.
[19] Y. Wang, B. J. Kim, B. Peng, W. Li, Y. Wang, M. Li, F. G. Omenetto, *Proc. Natl. Acad. Sci. U. S. A.* **2019**, *116*, 21361.
[20] Y. Tsuboi, M. Goto, A. Itaya, *J. Appl. Phys.* **2001**, *89*, 7917.
[21] R. Nozaki, S. Nakayama, M. Senna, *Thin Solid Films* **2013**, *542*, 214.
[22] D. Maniglio, W. Bonani, G. Bortoluzzi, E. Servoli, A. Motta, C. Migliaresi, *J. Bioact. Compat. Polym.* **2010**, *25*, 441.
[23] Z. Zhang, Y. Qu, X. Li, S. Zhang, Q. Wei, Y. Shi, L. Chen, *Appl. Surf. Sci.* **2014**, *303*, 255.
[24] X. Cheng, D. Deng, L. Chen, J. A. Jansen, S. G. C. Leeuwenburgh, F. Yang, *ACS Appl. Mater. Interfaces* **2020**, *12*, 12018.
[25] A. A. Valencia-Lazcano, R. Román-Doval, E. De La Cruz-Burelo, E. J. Millán-Casarrubias, A. Rodríguez-Ortega, *J. Biomed. Mater. Res., Part B* **2018**, *106*, 1655.
[26] P. Liu, G. Wang, Q. Ruan, K. Tang, P. K. Chu, *Bioact. Mater.* **2021**, *6*, 2134.
[27] Y. Cho, M. Lee, S. Park, Y. Kim, E. Lee, S. G. Im, *Biotechnol. Bioprocess Eng.* **2021**, *14*, 165.
[28] A. M. Trimukhe, K. N. Pandiyaraj, A. Tripathi, J. S. Melo, R. R. Deshmukh, *Advances in Biomaterials for Biomedical Applications*, Vol. *66*, Springer, Singapore **2017**.
[29] M. Narimisa, F. Krčma, Y. Onyshchenko, Z. Kozáková, R. Morent, N. De Geyter, *Polymers* **2020**, *12*, 354.
[30] S. Banerjee, E. Adhikari, P. Sapkota, A. Sebastian, S. Ptasinska, *Materials* **2020**, *13*, 2931.
[31] J. Kredl, J. Kolb, U. Schnabel, M. Polak, K. -D. Weltmann, K. Fricke, *Materials* **2016**, *9*, 274.
[32] A. Michelmore, P. Martinek, V. Sah, R. D. Short, K. Vasilev, *Plasma Processes Polym.* **2011**, *8*, 367.
[33] F. Arefi, V. Andre, P. Montazer-Rahmati, J. Amouroux, *Pure Appl. Chem.* **1992**, *64*, 715.
[34] N. V. Bhat, D. S. Wavhal, *Sep. Sci. Technol.* **2000**, *35*, 227.
[35] M. Macgregor, K. Vasilev, *Materials* **2019**, *12*, 191.
[36] C. Tendero, C. Tixier, P. Tristant, J. Desmaison, P. Leprince, *Spectrochim. Acta, Part B* **2006**, *61*, 2.
[37] X.-J. Lian, S. Wang, H. -S. Zhu, *Front. Mater. Sci. China* **2010**, *4*, 57.
[38] J. Ming, X. Li, J. Yang, D. Miao, X. Ning, *J. Textile Eng. Fashion Technol.* **2017**, *3*, 718.
[39] M. D. Chomachayi, A. Solouk, H. Mirzadeh, *Fibers Polym.* **2019**, *20*, 1594.
[40] S. Fajardo, F. R. García-Galvan, V. Barranco, J. C. Galvan, S. F. Batlle, *Trends Helicobacter pylori Infect.* **2016**, *1*, 13.
[41] G. S. Nadiger, N. V. Bhat, *J. Appl. Polym. Sci.* **1985**, *30*, 4127.
[42] C.-C. Chen, S. Riou, S. L. Hsu, H. D. Stidham, *Langmuir* **1996**, *12*, 1035.
[43] Y. Qi, H. Wang, K. Wei, Y. Yang, R. -Y. Zheng, I. Kim, K. -Q. Zhang, *Int. J. Mol. Sci.* **2017**, *18*, 237.
[44] Q. Lu, X. Hu, X. Wang, J. A. Kluge, S. Lu, P. Cebe, D. L. Kaplan, *Acta Biomater.* **2010**, *6*, 1380.
[45] Y. Cao, B. Wang, *Int. J. Mol. Sci.* **2009**, *10*, 1514.
[46] R. A. Hartvig, M. Van De Weert, J. Østergaard, L. Jorgensen, H. Jensen, *Langmuir* **2011**, *27*, 2634.
[47] R. A. Silva, M. D. Urzúa, D. F. S. Petri, P. L. Dubin, *Langmuir* **2010**, *26*, 14032.
[48] K. Terpilowski, D. Rymuszka, *Glass Phys. Chem.* **2016**, *42*, 535.
[49] S. Pinto, P. Alves, C. M. Matos, A. C. Santos, L. R. Rodrigues, J. A. Teixeira, M. H. Gil, *Colloids Surf., B* **2010**, *81*, 20.
[50] C. Yang, Y. J. Yuan, *Appl. Surf. Sci.* **2016**, *364*, 815.
[51] D. Bodas, C. Khan-Malek, *Sensors Actuators, B* **2007**, *123*, 368.
[52] N. Inagaki, S. Tasaka, K. Narushima, H. Kobayashi, *J. Appl. Polym. Sci.* **2002**, *85*, 2845.
[53] A. Vesel, M. Mozetic, *J. Phys.: Conf. Ser.* **2008**, *100*, 012027.
[54] J. C. M. Tavares, D. A. Cornélio, N. B. Da Silva, C. E. Bezerra De Moura, J. D. F. De Queiroz, J. C. Sá, C. A. Junior, S. R. B. De Medeiros, *Toxicology* **2009**, *262*, 138.
[55] C. B. Borkner, M. B. Elsner, T. Scheibel, *ACS Appl. Mater. Interfaces* **2014**, *6*, 15611.
[56] S. Popescu, M.-E. Zarif, C. Dumitriu, C. Ungureanu, C. Pirvu, *Coatings* **2020**, *10*, 518.
[57] A. Goudarzi, S. K. Sadrnezhaad, N. Johari, *Surf. Coat. Technol.* **2021**, *412*, 127001.
[58] S. Kaewpirom, S. Boonsang, *RSC Adv.* **2020**, *10*, 15913.
[59] C. Malinowski, F. He, Y. Zhao, I. Chang, D. W. Hatchett, S. Zhai, H. Zhao, *RSC Adv.* **2019**, *9*, 40792.
[60] A. Patelli, F. Mussano, P. Brun, T. Genova, E. Ambrosi, N. Michieli, G. Mattei, P. Scopece, L. Moroni, *ACS Appl. Mater. Interfaces* **2018**, *10*, 39512.
[61] A. Bucciarelli, T. Muthukumar, J. S. Kim, W. K. Kim, A. Quaranta, D. Maniglio, G. Khang, A. Motta, *ACS Biomater. Sci. Eng.* **2019**, *5*, 6374.
[62] A. Bucciarelli, S. Chiera, A. Quaranta, V. K. Yadavalli, A. Motta, D. Maniglio, *Adv. Funct. Mater.* **2019**, *29*, 1901134.
[63] P. B. Tooke, *TrAC, Trends Anal. Chem.* **1988**, *7*, 130.